Journal of Ultrafine Grained and Nanostructured Materials
https://jufgnsm.ut.ac.ir
Vol. 58, No.2, June 2025, pp. 197-207
Print ISSN: 2423-6845 Online ISSN: 2423-6837
DOI: 10.22059/jufgnsm.2025.02.05

Deformation-induced martensitic transformation kinetics in X5CrMnN17-8 austenitic stainless steel

Farideh Ansari, Hamed Mirzadeh *, Changiz Dehghanian

School of Metallurgy and Materials Engineering, College of Engineering, University of Tehran, Tehran, Iran

Recieved: 28 October 2025; Accepted: 15 November 2025

**Corresponding author, E-mail:* hmirzadeh@ut.ac.ir

ABSTRACT

Deformation-induced martensitic transformation kinetics for the X5CrMnN17-8 austenitic stainless steel was investigated and compared with the conventional grades of AISI 304 and AISI 201 stainless steels. It was revealed that cold rolling at room temperature results in the formation of α'-martensite, where the amount of α'-martensite increases with increasing reduction in thickness. It was observed that the X5CrMnN17-8 alloy has controlled deformation-induced martensitic transformation kinetics, which is faster than AISI 304 but slower than AISI 201 stainless steel. The famous Olson-Cohen, Guimaraes, Shin, Ahmedabadi, and Hill-based models, which are applicable for advanced high-strength steels with retained austenite and high-entropy alloys, were used to model the transformation kinetics during cold rolling. The advantages and limitations of each model were critically discussed and the model parameters were correlated with the stacking fault energy (SFE). It was concluded that the Shin and Ahmedabadi models have excellent accuracy; while the parameters of the Olson-Cohen and Hill-based models can perfectly be correlated with SFE as the base material parameter.

Keywords: *Austenitic stainless steels; Deformation-induced martensite; Phase transformation; Kinetic models; Stacking fault energy.*

1. Introduction

Austenitic stainless steels are ideal materials for a range of engineering applications because of their superior toughness, good weldability, and high resistance to corrosion [1,2]. Many of the austenitic stainless steels have metastable austenite, which transforms to martensite during deformation at around room temperature and cryogenic temperatures, resulting in a significant work hardening/transformation strengthening [3-5]. Moreover, the deformation-induced martensitic transformation can also be used for grain refinement [6,7]. Furthermore, the transformation-induced plasticity (TRIP) effect is one of basis of the advanced high-strength steels and high-performance high-entropy alloys [8-11]. Additionally, the formation of martensite via anneal hardening [12] is another important related aspect.

Accordingly, the kinetics of deformation-induced martensitic transformation is quite important when dealing with these stainless steels

[13,14]. The Olson-Cohen [15], Guimaraes [16], Shin [17], and Ahmedabadi [18], and Hill-based [19] models have been proposed for this purpose. Each model has its own advantages and limitations. Moreover, it is quite important to correlate the model parameters with the deformation conditions and the material parameters such as stacking fault energy (SFE).

Among different types of austenitic stainless steels, the low-Ni variants have garnered significant interest. The expensive nature of Ni and its negative impacts on the human body for biomedical uses led to the introduction of N-containing and Cr-Mn austenitic stainless steels with reduced Ni levels [20-23]. On the one hand, N-alloying is recognized as an effective technique for enhancing the solid solution strengthening impact [24-26]. On the other hand, substituting Ni with Mn reduces the stability of the austenite phase, promoting the deformation-induced martensitic transformation [27]. Moreover, the N-alloyed Cr-Mn austenitic stainless steels with reduced Ni levels have also been investigated by many researchers, including Hamada et al. [28], Souza Filho et al. [29], Gauss et al [30], and Tavares et al. [31], revealing a more appropriate deformation-induced martensitic transformation kinetics and good mechanical properties, which is quite important for mechanical properties. Therefore, investigating the kinetics of deformation-induced martensitic transformation in N-containing and Cr-Mn austenitic stainless steels with reduced Ni levels and comparison with conventional grades is quite important, which is the subject of the present work.

2. Experimental materials and procedures

As-received materials were the X5CrMnN17-8 sheet (0.093C-13.45Cr-1.30Ni-9.60Mn-0.150N, wt%), as a representative N-containing Cr-Mn austenitic stainless steel with reduced Ni level, as well as AISI 304 sheet (0.046C-17.91Cr-9.16Ni-1.54Mn-0.003N, wt%), as a representative conventional grade. The initial thickness of the sheets was 3 mm. Both alloys were received in the annealed condition with an average grain size of 30 μm and entirely austenitic microstructures. Cold rolling was performed in multiple passes at room temperature, with reductions in thickness in the range of 12.5 and 75%.

The preparation of the metallographic samples included electro-polishing (40 V, mixture of H_3PO_4-H_2SO_4) followed by electroetching (2 V, 60% HNO_3 solution) [32,33]. Subsequently, the microstructures were analyzed using an OLYMPUS VANOX optical microscope and a Mira3 Tescan scanning electron microscope (SEM).

A PHILIPS PW-3710 X-ray diffractometer (XRD) utilizing Cu-Kα radiation was used to track phase evolution during cold rolling. Moreover, based on the intensity of the diffraction peaks ($I_{(hkl)}$), Equation 1 [34,35] has been proposed for investigating the evolution of the deformation-induced martensite fraction ($f_{\alpha'}$) in stainless steels with promising outcomes:

$$f_{\alpha'} = I_{(211)\alpha'} / \{I_{(211)\alpha'} + 0.65(I_{(311)\gamma} + I_{(220)\gamma})\} \quad (1)$$

3. Results and discussion

3.1. Microstructural evolution and α'-martensite formation

Figures 1 depicts the microstructures of the as-received and cold rolled X5CrMnN17-8 stainless steel. An equiaxed microstructure with an average grain size of 30 μm can be seen for the as-received X5CrMnN17-8 sample; while cold rolling results in the elongation of grains, where this elongation increases with increasing the reduction in thickness. Moreover, as can be seen in the optical micrograph of the 12.5% rolled sample, the development of shear bands within the grains is evident. This aspect is more clearly observable in the high-magnification SEM image presented in the same figure. The intersections of the shear bands are recognized as the primary nucleation sites for the deformation-induced martensite [36,37].

While the optical micrographs show the development of the deformed microstructure, the XRD phase analysis is required to follow the phase evolutions during rolling, which is shown in Figures 2a for the X5CrMnN17-8 stainless steel and Figures 2b for the AISI 304 stainless steel. The XRD pattern for the as-received X5CrMnN17-8 stainless steel shown in Figures 2a reveals that this sample is fully austenitic. A minor degree of cold rolling (12.5%) led to the emergence of diffraction peaks corresponding to the deformation-induced martensite phases, which include α'-martensite and a tiny peak associated with the development of a small quantity of ε-martensite. These results are consistent with the microstructures of this sample in Figure 1, which show the appearance of shear band intersections for martensite nucleation. As the degree of deformation rises, the intensity of α'-martensite peaks grows; while that for the austenite decreases. Furthermore, with a significant thickness reduction of 75%, most peaks correspond to α'-martensite, and a minor peak of austenite is still observable ($f_{\alpha'}$ = 0.92 according to Equation 1). Similarly, for the AISI 304 stainless steel, Figures 2b reveals the formation of α'-martensite and increasing $f_{\alpha'}$ with increasing the reduction in thickness. At the reduction in thickness of 75%, $f_{\alpha'}$ = 0.88 according to Equation 1 can be calculated.

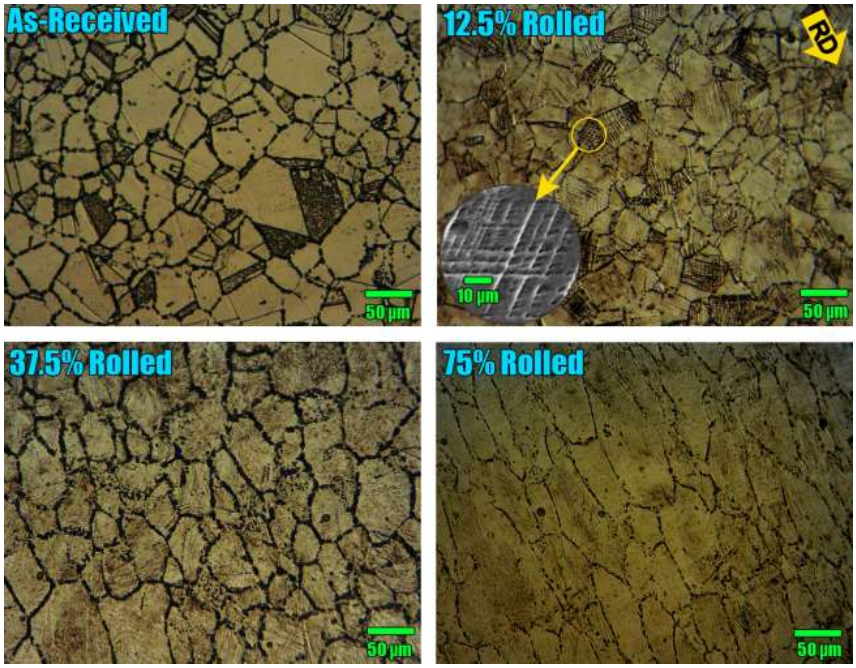

Fig. 1- Optical micrographs of the as-received and cold rolled X5CrMnN17-8 alloy and the SEM image of the 12.5% rolled sample. RD represents rolling direction for all of the micrographs.

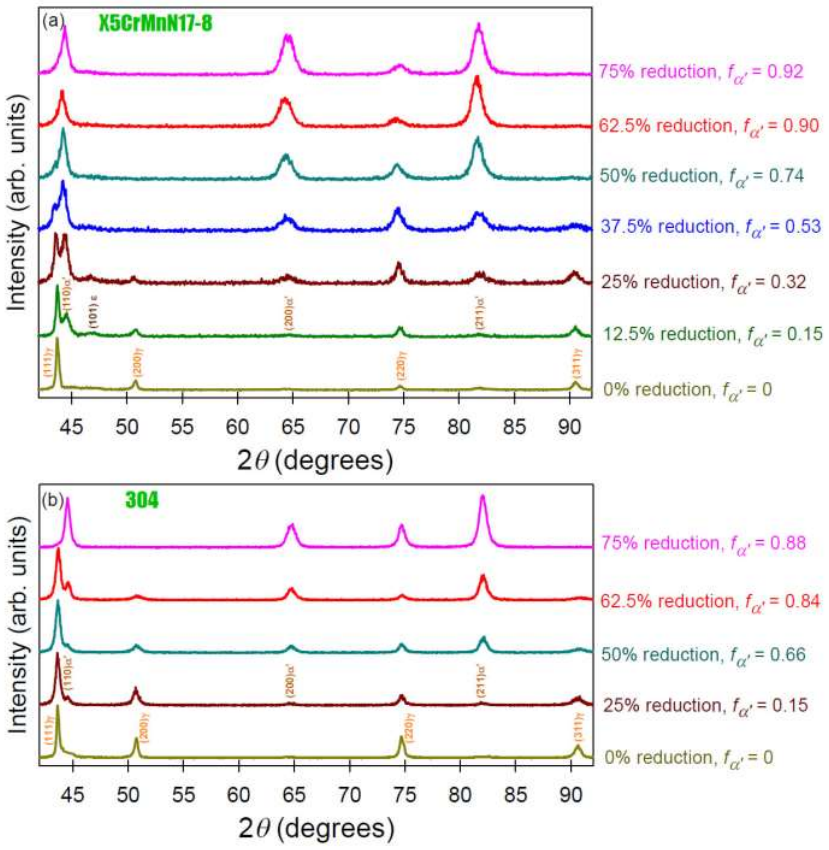

Fig. 2- XRD patterns of as-received and cold rolled (a) X5CrMnN17-8 and (b) AISI 304 stainless steels.

To compare the kinetics of α'-martensite formation in X5CrMnN17-8 and AISI 304 stainless steels, the plots of $f_{\alpha'}$ versus equivalent strain is usually used. In rolling, $\varepsilon_{thickness} = \ln(1/(1-r))$, where r is the reduction in thickness. Constancy of volume during plastic flow gives $\varepsilon_{longitudinal} + \varepsilon_{thickness} + \varepsilon_{width} = 0$. For the plane-strain rolling, $\varepsilon_{width} = 0$, and hence, $\varepsilon_{longitudinal} = -\varepsilon_{thickness}$. Accordingly, the equivalent strain can be calculated using equation 2.

The plots of $f_{\alpha'}$ versus equivalent strain for both X5CrMnN17-8 and AISI 304 stainless steels are depicted in Figure 3. Since the XRD analysis was performed three times for each sample, the results are reliable, which can be conformed by the small error bars shown in Figure 3. Moreover, according to the research conducted by Sadeghpour et al. [38], the plot for a highly-metastable alloy (AISI 201 stainless steel (0.025C-16.73Cr-4.3Ni-7.2Mn-0.12Ti, wt%) have also been included. The X5CrMnN17-8 and AISI 304 stainless steels ultimately achieve approximately 90 vol% α'-martensite; while the AISI 201 stainless steel rapidly attains about 100 vol% α'-martensite at low strains. To uncover this behavior, SFE of these stainless steels may be examined. For this purpose, based on the mass percents of alloying elements, the Dai formula (Equation 3) can be used [27,39].

Considering the previously stated chemical compositions, the SFE values for AISI 201, X5CrMnN17-8, and AISI 304 stainless steels can be computed using Equation 3 as 11.22, 15.64, and 23.08 mJ/m^2, respectively. Thus, reducing SFE leads to a notable increase in the kinetics of α'-martensite formation, which aligns with the expectations [40-42].

For each alloy, $f_{\alpha'}$ rises in a sigmoidal fashion as the equivalent rolling strain increases. However, the kinetics of α'-martensite is different, which is investigated in the next section using different models.

$$\bar{\varepsilon} = \sqrt{(\varepsilon_{longitudinal}^2 + \varepsilon_{thickness}^2 + \varepsilon_{width}^2) \times 2/3} = 1.1547 \ln(1/(1-r)) \quad (2)$$

$$\mathrm{SFE(mJ/m^2)} = 39 + 1.59Ni - 1.34Mn + 0.06Mn^2 - 1.75Cr + 0.01Cr^2 + 15.21Mo - 5.59Si$$
$$- 60.69\sqrt{C + 1.2N} + 26.27(C + 1.2N)\sqrt{Cr + Mn + Mo} + 0.61\sqrt{Ni(Cr + Mn)} \quad (3)$$

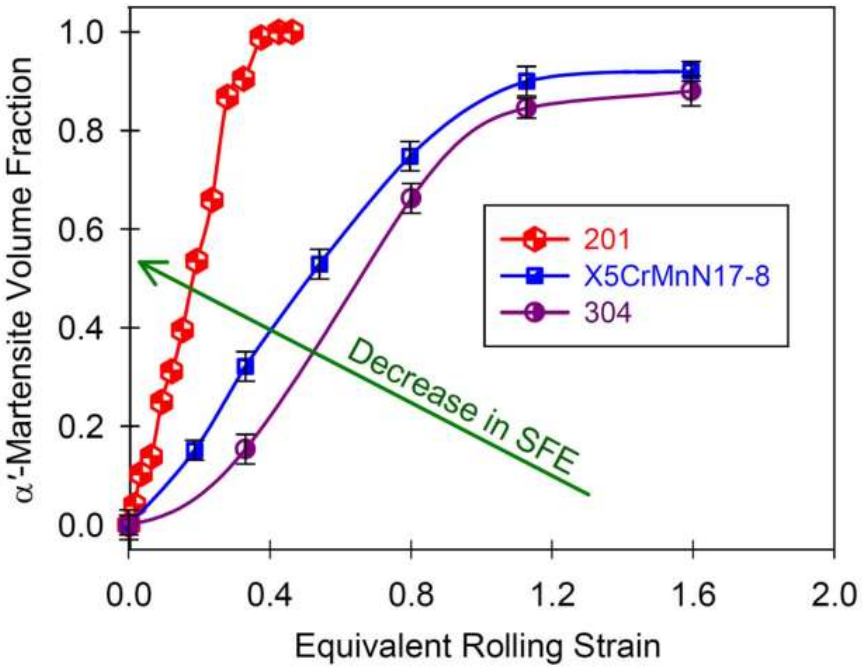

Fig. 3- Evolution of α'-martensite content during rolling for the X5CrMnN17-8 and AISI 304 stainless steels as well as AISI 201 stainless steel (data taken from [38]).

3.2. Kinetics of α'-martensite formation

To evaluate the transformation kinetics, firstly, the well-known Olson-Cohen model (Equation 4) [15] was considered:

$$f_{\alpha'} = 1 - \exp\{-\beta\{1 - \exp(-\alpha\varepsilon_{eq})\}^n\} \quad (4)$$

where α is associated with the shear-band formation rate, β represents the likelihood that an intersection of shear bands will produce a martensitic embryo, and n is a constant exponent (4.5 for austenitic stainless steels [15,43,44]). The plots for all three stainless steels are depicted in Figure 4a. It can be seen that the Olson-Cohen model is able to illustrate the sigmoidal kinetics of α'-martensite formation.

The obtained α and β values based on the non-linear regression analysis are summarized in Figure 4b versus SFE. It is observable that α decreases by increasing SFE, suggesting that the rate of shear-band formation decreases with increasing SFE, consistent with the previous investigations [15,44]. However, β does not show any distinct trend.

Guimaraes [16] utilized the Johnson–Mehl–Avrami–Kolmogorov (JMAK) model to examine the kinetics of α'-martensite formation by replacing time with strain (Equation 5), where n and K represent parameters related to the nucleation mode and the nucleation and growth rates, respectively [16,44]:

$$f_{\alpha'} = 1 - \exp\{-K\varepsilon^n\} \quad (5)$$

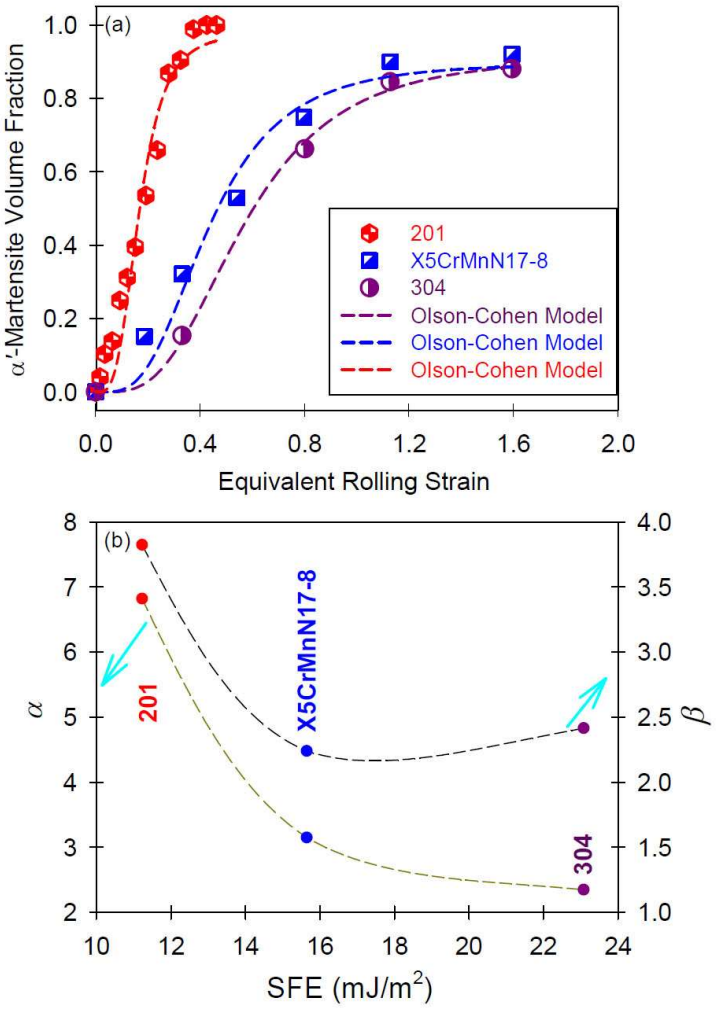

Fig. 4- (a) Olson-Cohen model applied for investigating the transformation kinetics and (b) summary of model parameters versus SFE.

The plots for all three stainless steels are depicted in Figure 5a. It can be seen that the outcomes of the Guimaraes model are acceptable. However, contrary to the Olson-Cohen model, in the Guimaraes model, $f_{\alpha'}$ eventually attain the value of 1, which is not consistent with the behavior seen for the X5CrMnN17-8 and AISI 304 stainless steels, where $f_{\alpha'}$ saturates at ~0.9. The obtained n and K values based on the non-linear regression analysis are summarized in Figure 5b versus SFE. It is observable that n does not change considerably, as it is related to the nucleation mode. However, K generally decreases by increasing SFE, indicating the slower kinetics of α'-martensite formation, confirming the usefulness of this model; although this decrease is not pronounced when comparing the X5CrMnN17-8 and AISI 304 stainless steels.

Shin et al. [17] introduced the saturated $f_{\alpha'}$ (f_{sat}), the critical inelastic strain at which the accumulated internal strain energy is sufficient to compensate for the driving force deficit for α'-martensite formation (ε_0), the austenite stability parameter (λ), and deformation mode exponent (m):

$$f_{\alpha'} / f_{sat} = 1 - \exp\{-\lambda(\varepsilon - \varepsilon_0)^m\} \quad (6)$$

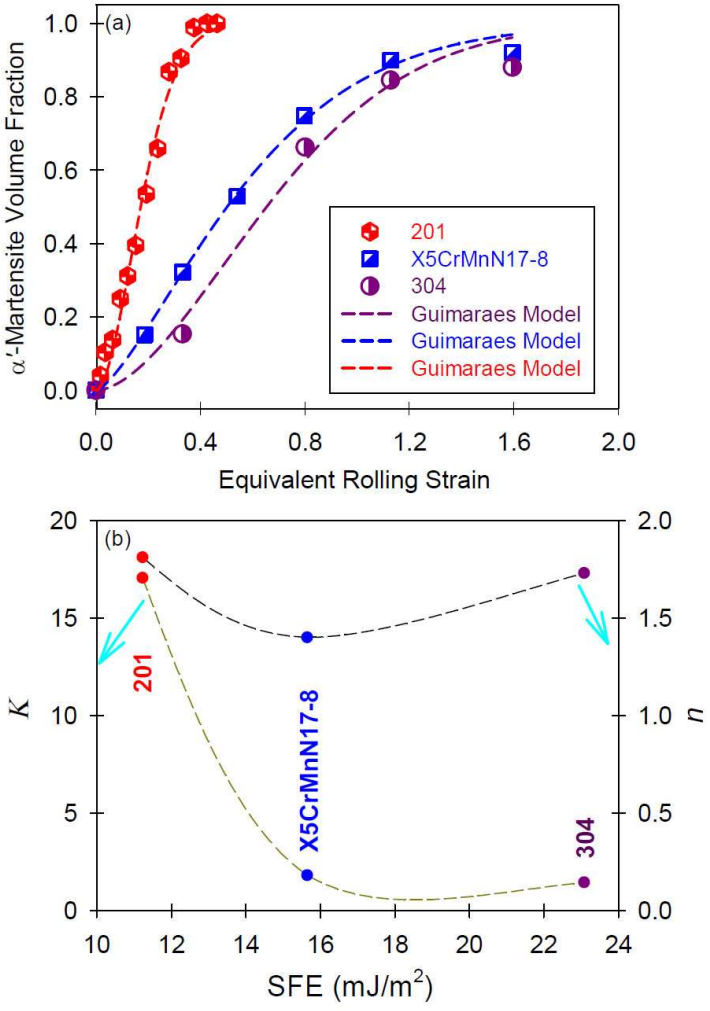

Fig. 5- (a) Guimaraes model applied for investigating the transformation kinetics and (b) summary of model parameters versus SFE.

The plots for all three stainless steels are depicted in Figure 6a. The results are quite promising. The obtained λ and m values based on the non-linear regression analysis are summarized in Figure 6b versus SFE. It is noteworthy that for all three stainless steels, ε_0 was obtained as 0 during the fitting. It is observable that λ, as the austenite stability parameter, is dependent on the SFE value; demonstrating the usefulness of this model for evaluating the austenite stability. However, this decrease is not pronounced when comparing the X5CrMnN17-8 and AISI 304 stainless steels. Moreover, m, as the deformation mode exponent, for different metastable HEAs is different. Anyway, this model is an improved JMAK model, which resolved the problem of $f_{\alpha'}$ saturation by introducing f_{sat}.

Ahmedabadi et al. [18] proposed Equation 7 by introducing the strain associated with the maximum rate of transformation (ε_{max}) and the transformation rate parameter (η):

$$f_{sat} / f_{\alpha'} = 1 + \exp\{-\eta(\varepsilon - \varepsilon_{\max})\} \quad (7)$$

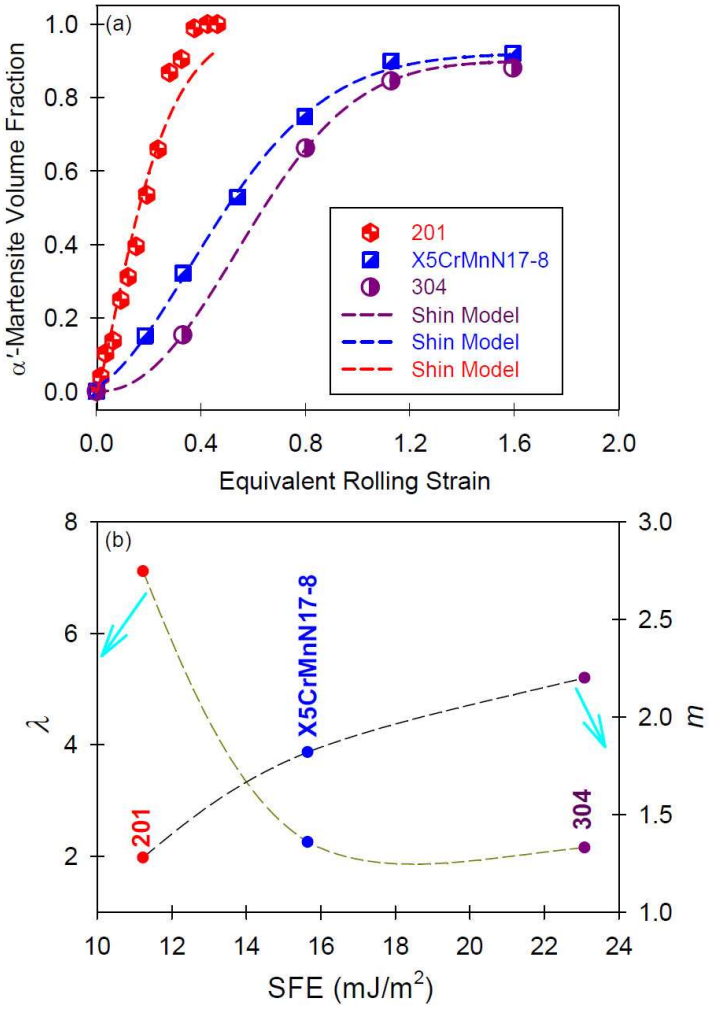

Fig. 6- (a) Shin model applied for investigating the transformation kinetics and (b) summary of model parameters versus SFE.

The plots for all three stainless steels are depicted in Figure 7a. The fitting of the model is excellent. The obtained ε_{max} and η values based on the non-linear regression analysis are summarized in Figure 7b versus SFE. It can be seen that, η, as the transformation rate parameter, decreases with increasing SFE, revealing that α'-martensite formation becomes slower. However, this decrease is not pronounced when comparing the X5CrMnN17-8 and AISI 304 stainless steels. On the other hand, ε_{max} clearly increases with increasing SFE, which is quite promising.

Recently, Sohrabi et al. [19] proposed the Hill-based model (Equation 8) by adding the p and q parameters, where χ = p × q was considered as the sole austenite stability parameter:

$$f_{\alpha'} / f_{sat} = 1 - p/(p + \varepsilon_{eq}^{q}) \quad (8)$$

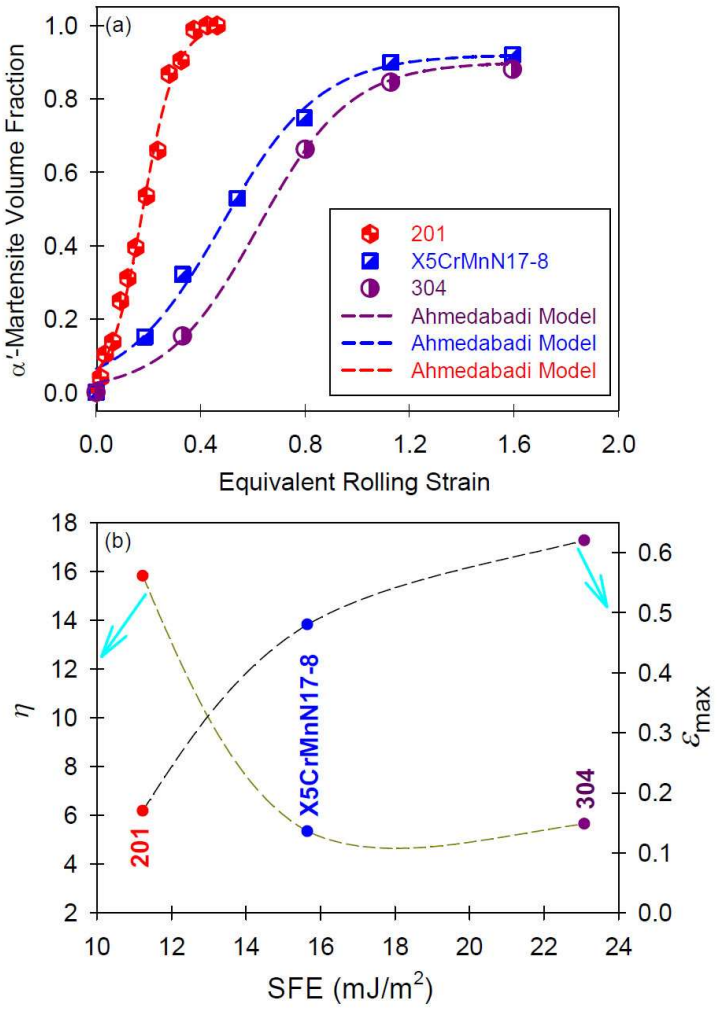

Fig. 7- (a) Ahmedabadi model applied for investigating the transformation kinetics and (b) summary of model parameters versus SFE.

The plots for all three stainless steels are depicted in Figure 8a. The fitting of the model is reasonably well. The obtained p, q, and χ = p × q values based on the non-linear regression analysis are summarized in Figure 8b versus SFE. It can be seen that, χ, as the austenite stability parameter, increases with increasing SFE, revealing that α'-martensite formation becomes slower. Therefore, χ is highly dependent on SFE, and it is an appropriate parameter to describe the kinetics of α'-martensite formation.

It is possible to compare the ability of these techniques in modeling the kinetics of α'-martensite formation via applying the root mean square error [45-47]:

$$\mathrm{RMSE} = \sqrt{(1/N)\sum_{i=1}^{N}(x_i^{\mathrm{Model}} - x_i^{\mathrm{Experiment}})^2} \qquad (9)$$

The RMSE values for the Olson-Cohen, Guimaraes, Shin, Ahmedabadi, and Hill-based models were determined as 7.3, 6.3, 5.5, 5.1, and 7.3% respectively, revealing the good accuracy of the Shin and Ahmedabadi models. On the other hand, while the accuracy of the Hill-based model is similar to the Olson-Cohen one, the correlation of the parameters of these two models, especially χ, with the governing material parameter (SFE in this case) is quite promising. In summary, all parameters of the discussed models are plausibly explained by the SFE value and it is possible to regulate α'-martensite formation kinetics by tuning the SFE.

Regarding the investigated stainless steels in the present work, a significant difference in the kinetic

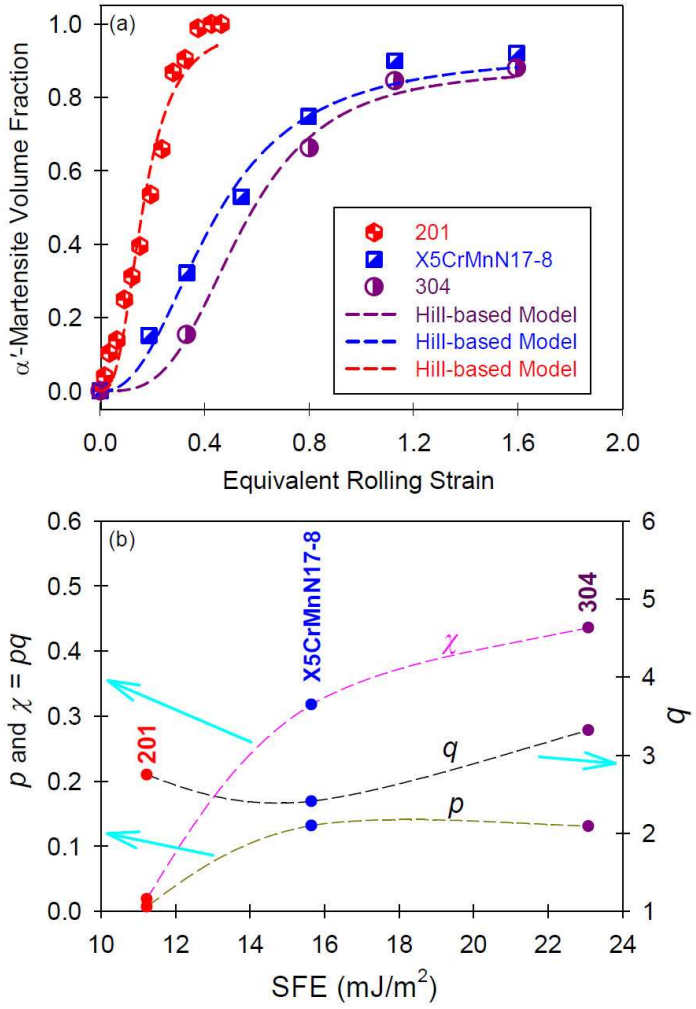

Fig. 8- (a) Hill-based model applied for investigating the transformation kinetics and (b) summary of model parameters versus SFE.

parameters between the AISI 201 alloy and other stainless steels was observed, which is linked to the extremely high metastability of the austenite phase present in this alloy. The X5CrMnN17-8 alloy benefits from a higher Mn content while reducing Ni content, resulting in greater metastability than the AISI 304 stainless steel. Nevertheless, the X5CrMnN17-8 alloy possesses a greater concentration of C and also has a significant amount of N (both serve as austenite stabilizers [48-50]), leading to a more subtle metastability in the X5CrMnN17-8 alloy.

4. Summary

The kinetics of deformation-induced martensitic transformation for the X5CrMnN17-8 austenitic stainless steel during cold rolling was examined and compared with conventional grades of AISI 304 and AISI 201 stainless steels. It was discovered that cold rolling at room temperature leads to the emergence of α'-martensite in the microstructure, with the quantity of α'-martensite growing as the reduction in thickness rises. It was noted that the X5CrMnN17-8 alloy exhibits regulated kinetics of deformation-induced martensitic transformation, which is quicker than AISI 304 but slower than AISI 201 stainless steel. The renowned Olson-Cohen, Guimaraes, Shin, and Ahmedabadi, along with Hill-based models were utilized to model the transformation kinetics throughout cold rolling. The benefits and drawbacks of each model were thoroughly examined, and the model parameters were linked to the stacking fault energy (SFE). The final concluding remark is that the Shin and Ahmedabadi models demonstrate outstanding accuracy, while the parameters of the Olson-Cohen and Hill-based models can be perfectly correlated with SFE as the fundamental material parameter. In this regard, it was revealed that the sole austenite stability parameter, χ, in the Hill-based model of $f_{\alpha'}/f_{sat}=1-p(p+\varepsilon_{eq}^{q})$ is quite promising for comparison purposes.

References

1. Sohrabi, M.J., Mirzadeh, H. and Dehghanian, C., 2020. Significance of martensite reversion and austenite stability to the mechanical properties and transformation-induced plasticity effect of austenitic stainless steels. Journal of Materials Engineering and Performance, 29(5), pp.3233-3242.
2. Shirdel, M., Mirzadeh, H. and Habibi Parsa, M., 2014. Microstructural evolution during normal/abnormal grain growth in austenitic stainless steel. Metallurgical and Materials Transactions A, 45(11), pp.5185-5193.
3. Kishore, K., Kumar, R.G. and Chandan, A.K., 2021. Critical assessment of the strain-rate dependent work hardening behaviour of AISI 304 stainless steel. Materials Science and Engineering: A, 803, p.140675.
4. Huang, M., Wang, L., Yuan, S., Wang, J., Wang, C., Mogucheva, A. and Xu, W., 2022. Scale-up fabrication of gradient AGS in austenitic stainless steels achieves a simultaneous increase in strength and toughness. Materials Science and Engineering: A, 853, p.143763.
5. Parnian, P., Parsa, M.H., Mirzadeh, H. and Jafarian, H.R., 2017. Effect of drawing strain on development of martensitic transformation and mechanical properties in AISI 304L stainless steel wire. Steel Research International, 88(8), p.1600423.
6. W. Qin, J. Li, Y. Liu, J. Kang, L. Zhu, D. Shu, P. Peng, D. She, D. Meng, Y. Li, Effects of grain size on tensile property and fracture morphology of 316L stainless steel, Materials Letters 254 (2019) 116-119.
7. Li, J., Gao, B., Huang, Z., Zhou, H., Mao, Q. and Li, Y., 2018. Design for strength-ductility synergy of 316L stainless steel with heterogeneous lamella structure through medium cold rolling and annealing. Vacuum, 157, pp.128-135.
8. Azizi, G., Mirzadeh, H. and Parsa, M.H., 2015. Dependency of deformation behavior of retained austenite in TRIP steels on microstructural and chemical homogeneity. Acta Metallurgica Sinica (English Letters), 28(10), pp.1272-1277.
9. Deldar, S., Mirzadeh, H. and Parsa, M.H., 2017. Toward unraveling the importance of deformed microstructure before TRIP heat treatment in transformation-induced plasticity steels. Steel Research International, 88(5), p.1600275.
10. Jalali, A., Mehranpour, M.S., Kalhor, A., Sohrabi, M.J., Heydarinia, A., Hasnabadi, F., Mirzadeh, H., Malekan, M., Sarkari Khorrami, M., Fallah, V. and Rodak, K., 2025. Superior strength-ductility synergy in metastable high-entropy alloys: the crucial role of FCC to BCC martensitic phase transformation. Journal of Alloys and Compounds, 1044, p.184464.
11. Khorrami, M., Hanzaki, A.Z., Abedi, H.R., Moallemi, M., Mola, J. and Chen, G., 2021. On the effect of Mn-content on the strength-ductility balance in Ni-free high N transformation induced plasticity steels. Materials Science and Engineering: A, 814, p.141260.
12. Z. Zhou, S. Wang, J. Li, Y. Li, X. Wu, Y. Zhu, Hardening after annealing in nanostructured 316L stainless steel, Nano Materials Science 2 (2020) 80-82.
13. Jain, A. and Varshney, A., 2024. A critical review on deformation-induced transformation kinetics of austenitic stainless steels. Materials Science and Technology, 40(2), pp.75-106.
14. Tiwari, P. and Varshney, A., 2024. A Review on Measurement Techniques of Deformation-Induced Transformation Kinetics in Transformation-Induced Plasticity and Transformation-Induced Plasticity-Assisted Steels. steel research international, 95(1), p.2300341.
15. Olson, G.B. and Cohen, M., 1975. Kinetics of strain-induced martensitic nucleation. Metallurgical transactions A, 6, pp.791-795.
16. Guimaraes, J.R.C., 1972. The deformation-induced martensitic reaction in polycrystalline Fe-30.7 Ni-0.06 C. Scripta Metallurgica, 6(9), pp.795-798.
17. Shin, H.C., Ha, T.K. and Chang, Y.W., 2001. Kinetics of deformation induced martensitic transformation in a 304 stainless steel. Scripta Materialia, 45(7), pp.823-829.
18. Ahmedabadi, P.M., Kain, V. and Agrawal, A., 2016. Modelling kinetics of strain-induced martensite transformation during plastic deformation of austenitic stainless steel. Materials & Design, 109, pp.466-475.
19. Sohrabi, M.J., Mehranpour, M.S., Heydarinia, A., Kalhor, A., Lee, J.H., Mirzadeh, H., Mahmudi, R., Parsa, M.H., Rodak, K. and Kim, H.S., 2024. Deformation-induced martensitic transformation kinetics in TRIP-assisted steels and high-entropy alloys. Acta Materialia, 280, p.120354.
20. Chen, S., Wang, Q., Yang, H. and Yang, K., 2023. High-Nitrogen Nickel-Free Stainless Steel: An Attractive Material with Potential for Biomedical Application. steel research international, 94(10), p.2200355.
21. Kumar, C.S., Singh, G., Poddar, S., Varshney, N., Mahto, S.K., Podder, A.S., Chattopadhyay, K., Rastogi, A., Singh, V. and

Mahobia, G.S., 2021. High-manganese and nitrogen stabilized austenitic stainless steel (Fe–18Cr–22Mn–0.65 N): a material with a bright future for orthopedic implant devices. Biomedical Materials, 16(6), p.065011.
22. Chatterjee, D., 2021. Effect of repeated warm rolling cold rolling and annealing on the microstructure and mechanical properties of AISI 301LN grade austenitic stainless steel. Materials Today: Proceedings, 46, pp.10604-10611.
23. Rezayat, M., Moradi, M. and Mateo, A., 2024. Nanosecond multi-passes laser surface texturing on AISI 301LN TRIP steel. The International Journal of Advanced Manufacturing Technology, 132(9), pp.4753-4764.
24. Wang, Y., Wang, Z., Wang, W. and Ma, B., 2023. Effect of nitrogen content on mechanical properties of 316L (N) austenitic stainless steel. Materials Science and Engineering: A, 884, p.145549.
25. Saravanan, P., Govindaraj, Y., Khalkho, B., Srikanth, S., Kumar, V. and Neelakantan, L., 2023. Mechanical properties and corrosion behaviour of developed high nitrogen high manganese stainless steels. Materialwissenschaft und Werkstofftechnik, 54(5), pp.615-626.
26. Zhang, Y., Li, M., Bi, H., Gu, J., Chen, D., Chang, E. and Zhang, W., 2018. Martensite transformation behavior and mechanical properties of cold-rolled metastable Cr-Mn-Ni-N austenitic stainless steels. Materials Science and Engineering: A, 724, pp.411-420.
27. Sohrabi, M.J., Naghizadeh, M. and Mirzadeh, H., 2020. Deformation-induced martensite in austenitic stainless steels: A review. Archives of Civil and Mechanical Engineering, 20, pp.1-24.
28. Hamada, A.S., Karjalainen, L.P., Misra, R.D.K. and Talonen, J., 2013. Contribution of deformation mechanisms to strength and ductility in two Cr–Mn grade austenitic stainless steels. Materials Science and Engineering: A, 559, pp.336-344.
29. Souza Filho, I.R.D., Zilnyk, K.D., Sandim, M.J.R., Bolmaro, R.E. and Sandim, H.R.Z., 2017. Strain partitioning and texture evolution during cold rolling of AISI 201 austenitic stainless steel. Materials Science and Engineering: A, 702, pp.161-172.
30. Gauss, C., Souza Filho, I.R., Sandim, M.J.R., Suzuki, P.A., Ramirez, A.J. and Sandim, H.R.Z., 2016. In situ synchrotron X-ray evaluation of strain-induced martensite in AISI 201 austenitic stainless steel during tensile testing. Materials Science and Engineering: A, 651, pp.507-516.
31. Tavares, S.S.M., Pardal, J.M., Da Silva, M.G., Abreu, H.F.G.D. and da Silva, C.R., 2009. Deformation induced martensitic transformation in a 201 modified austenitic stainless steel. Materials characterization, 60(8), pp.907-911.
32. Ansari, F., Mirzadeh, H. and Dehghanian, C., 2025. Strain-induced martensite formation and mechanical properties of a low-Ni N-containing Cr–Mn austenitic stainless steel. Journal of Materials Research and Technology, 36, pp.1504-1510.
33. Naghizadeh, M. and Mirzadeh, H., 2016. Elucidating the effect of alloying elements on the behavior of austenitic stainless steels at elevated temperatures. Metallurgical and Materials Transactions A, 47, pp.5698-5703.
34. B. Fultz, J. Howe, Transmission electron microscopy and diffractometry of materials, 3rd ed., Springer, Berlin, Germany, 2008.
35. Sohrabi, M.J., Mirzadeh, H., Sadeghpour, S. and Mahmudi, R., 2023. Grain size dependent mechanical behavior and TRIP effect in a metastable austenitic stainless steel. International Journal of Plasticity, 160, p.103502.
36. Talonen, J. and Hänninen, H., 2007. Formation of shear bands and strain-induced martensite during plastic deformation of metastable austenitic stainless steels. Acta Materialia, 55(18), pp.6108-6118.
37. Olson, G.B. and Cohen, M., 1972. A mechanism for the strain-induced nucleation of martensitic transformations. Journal of the Less Common Metals, 28(1), pp.107-118.
38. Sadeghpour, S., Kermanpur, A. and Najafizadeh, A., 2013. Influence of Ti microalloying on the formation of nanocrystalline structure in the 201L austenitic stainless steel during martensite thermomechanical treatment. Materials Science and Engineering: A, 584, pp.177-183.
39. Dai, Q.X., Wang, A.D., Cheng, X.N., Luo, X.M., 2002. Stacking fault energy of cryogenic austenitic steels. Chinese Physics, 11(6), p.596.
40. Lo, K.H., Shek, C.H. and Lai, J.K.L., 2009. Recent developments in stainless steels. Materials Science and Engineering: R: Reports, 65(4-6), pp.39-104.
41. Mehranpour, M.S., Sohrabi, M.J., Kalhor, A., Lee, J.H., Heydarinia, A., Mirzadeh, H., Sadeghpour, S., Rodak, K., Nili-Ahmadabadi, M., Mahmudi, R. and Kim, H.S., 2024. Exceptional strength-ductility synergy in the novel metastable FeCoCrNiVSi high-entropy alloys via tuning the grain size dependency of the transformation-induced plasticity effect. International Journal of Plasticity, 182, p.104115.
42. Mehranpour, M.S., Sohrabi, M.J., Jalali, A., Kalhor, A., Heydarinia, A., Aghdam, M.Z., Mirzadeh, H., Malekan, M., Shahmir, H., Rodak, K. and Kim, H.S., 2025. Coupling different strengthening mechanisms with transformation-induced plasticity (TRIP) effect in advanced high-entropy alloys: a comprehensive review. Materials Science and Engineering: A, p.147914.
43. Mohammadzehi, S. and Mirzadeh, H., 2024. Grain refinement of austenitic stainless steels by cross rolling and annealing treatment: A review. Journal of Ultrafine Grained and Nanostructured Materials, 57(2), pp.112-119.
44. Naghizadeh, M. and Mirzadeh, H., 2018. Modeling the kinetics of deformation-induced martensitic transformation in AISI 316 metastable austenitic stainless steel. Vacuum, 157, pp.243-248.
45. Alibeyki, M., Mirzadeh, H., Najafi, M. and Kalhor, A., 2017. Modification of rule of mixtures for estimation of the mechanical properties of dual-phase steels. Journal of Materials Engineering and Performance, 26(6), pp.2683-2688.
46. Montazeri-Pour, M., Parsa, M.H. and Mirzadeh, H., 2014. Constitutive description of severely deformed metals based on dimensional analysis. Materials Science and Technology, 30(6), pp.719-724.
47. Gharechomaghlu, M. and Mirzadeh, H., 2020. Computational evaluation of the homogeneity of composites processed by accumulative roll bonding (ARB). Journal of Computational & Applied Research in Mechanical Engineering (JCARME), 9(2), pp.351-358.
48. Behjati, P., Kermanpur, A., Najafizadeh, A., Samaei Baghbadorani, H., Karjalainen, L.P., Jung, J.G. and Lee, Y.K., 2014. Effect of nitrogen content on grain refinement and mechanical properties of a reversion-treated Ni-free 18Cr-12Mn austenitic stainless steel. Metallurgical and Materials Transactions A, 45, pp.6317-6328.
49. Zhang, Y., Wang, C., Reddy, K.M., Li, W. and Wang, X., 2022. Study on the deformation mechanism of a high-nitrogen duplex stainless steel with excellent mechanical properties originated from bimodal grain design. Acta Materialia, 226, p.117670.
50. Das, A., 2016. Revisiting stacking fault energy of steels. Metallurgical and Materials Transactions A, 47, pp.748-768.